

The neutron star transient and millisecond pulsar in M28: from sub-luminous accretion to rotation-powered quiescence

Manuel Linares^{1,2*}, Arash Bahramian³, Craig Heinke³, Rudy Wijnands⁴,
Alessandro Patruno^{5,6}, Diego Altamirano^{4,7}, Jeroen Homan⁸, Slavko Bogdanov⁹,
David Pooley^{10,11}

¹ Instituto de Astrofísica de Canarias, c/ Vía Láctea s/n, E-38205 La Laguna, Tenerife, Spain

² Universidad de La Laguna, Departamento de Astrofísica, E-38206 La Laguna, Tenerife, Spain

³ Department of Physics, University of Alberta, CCIS 4-183, Edmonton, AB T6G 2E1, Canada

⁴ Astronomical Institute “Anton Pannekoek”, University of Amsterdam, Science Park 904, 1098XH Amsterdam, The Netherlands

⁵ Leiden Observatory, Leiden University, PO Box 9513, 2300RA Leiden, The Netherlands

⁶ ASTRON, The Netherlands Institute for Radio Astronomy, Postbus 2, 7990-AA Dwingeloo, The Netherlands

⁷ Physics & Astronomy, University of Southampton, Southampton, Hampshire SO17 1BJ, UK

⁸ Kavli Institute for Astrophysics and Space Research, Massachusetts Institute of Technology, 70 Vassar Street, Cambridge, MA 02139, USA

⁹ Columbia Astrophysics Laboratory, Columbia University, 550 West 120th Street, New York, NY 10027, USA

¹⁰ Department of Physics, Sam Houston State University, Huntsville, TX, USA

¹¹ Eureka Scientific, Austin, TX, USA

Accepted 2013 November 6. Received 2013 October 14; in original form 2013 September 4.

ABSTRACT

The X-ray transient IGR J18245–2452 in the globular cluster M28 contains the first neutron star (NS) seen to switch between rotation-powered and accretion-powered pulsations. We analyse its 2013 March–April 25 d-long outburst as observed by *Swift*, which had a peak bolometric luminosity of $\sim 6\%$ of the Eddington limit (L_{Edd}), and give detailed properties of the thermonuclear burst observed on 2013 April 7. We also present a detailed analysis of new and archival *Chandra* data, which we use to study quiescent emission from IGR J18245–2452 between 2002 and 2013. Together, these observations cover almost five orders of magnitude in X-ray luminosity (L_X , 0.5–10 keV). The *Swift* spectrum softens during the outburst decay (photon index Γ from 1.3 above $L_X/L_{Edd}=10^{-2}$ to ~ 2.5 at $L_X/L_{Edd}=10^{-4}$), similar to other NS and black hole (BH) transients. At even lower luminosities, $L_X/L_{Edd}=[10^{-4}-10^{-6}]$, deep *Chandra* observations reveal hard ($\Gamma=1-1.5$), purely non-thermal and highly variable X-ray emission in quiescence. We therefore find evidence for a spectral transition at $L_X/L_{Edd}\sim 10^{-4}$, where the X-ray spectral softening observed during the outburst decline turns into hardening as the source goes to quiescence. Furthermore, we find a striking variability pattern in the 2008 *Chandra* light curves: rapid switches between a high-luminosity “active” state ($L_X \simeq 3.9 \times 10^{33}$ erg s⁻¹) and a low-luminosity “passive” state ($L_X \simeq 5.6 \times 10^{32}$ erg s⁻¹), with no detectable spectral change. We put our results in the context of low luminosity accretion flows around compact objects and X-ray emission from millisecond radio pulsars. Finally, we discuss possible origins for the observed mode switches in quiescence, and explore a scenario where they are caused by fast transitions between the magnetospheric accretion and pulsar wind shock emission regimes.

Key words: X-rays: bursts — X-rays: individual (IGR J18245–2452) — stars: neutron — X-rays: binaries — globular clusters: individual(M28) — pulsars: individual(PSR J1824–2452I)

1 INTRODUCTION

Globular clusters have proved to be excellent locations for the study of low-mass X-ray binaries (LMXBs). This is due in part to the dynamical production of LMXBs through stellar interactions, which enhances the number of LMXBs per unit stellar mass by a factor of ~ 100 over the rest of the Galaxy (e.g., Clark 1975), and makes clusters excellent targets to identify and study LMXBs. The knowledge of the companion's age and metallicity, and the tight constraints on the distance and the absorbing column density (N_H) provided by optical observations, also assist in studies of LMXBs in clusters (e.g. Kuulkers et al. 2003).

Eighteen luminous (0.5–10 keV luminosity $L_X > 10^{35}$ erg s $^{-1}$) LMXBs have been reported to date in 15 Galactic globular clusters (including IGR J18245–2452). In all cases the accreting compact object has been identified as a neutron star (NS), mostly thanks to the detection of thermonuclear bursts (in 16 systems) or accretion-powered pulsations (in 4 systems). About half are transients, detectable in outburst with wide-field X-ray monitors for a few days to months (see Table 5 in Bahramian et al. 2013, and references therein). Most LMXBs in globular clusters are usually in deep quiescence ($L_X < 10^{33}$ erg s $^{-1}$), undergoing little or no accretion. An estimated total of ~ 200 quiescent LMXBs exist in the Galactic globular cluster system, identified through deep observations with the high-resolution Chandra satellite (Pooley et al. 2003; Heinke, Grindlay & Edmonds 2005). Quiescent NS-LMXBs typically produce blackbody-like thermal emission from their surfaces at $L_X \sim 10^{32-33}$ erg s $^{-1}$ (Rutledge et al. 2000), although a substantial subset of quiescent NS-LMXB spectra are dominated by non-thermal emission of unknown origin, perhaps produced by continued low-level accretion or a pulsar wind shock (Campana et al. 1998; Wijnands et al. 2005). The thermal NS surface emission is understood to be due to the release of heat deposited in the deep crust during accretion outbursts (Brown, Bildsten & Rutledge 1998; Rutledge et al. 2002).

The globular cluster M28 (NGC 6626) is home to 12 known millisecond radio pulsars (MRPs, Begin 2006; Bogdanov et al. 2011b). Numerous other faint X-ray sources in the cluster were identified with deep *Chandra*-ACIS observations in 2002 and 2008, including a relatively bright source (S26) with a soft spectrum indicative of a quiescent NS-LMXB (Becker et al. 2003; Servillat et al. 2012). An unusual, subluminescent (~ 0.02 of the Eddington luminosity) X-ray burst was detected from the direction of M28's core by ASCA, during a time when no LMXB was obviously active in the cluster, suggesting low-level accretion in quiescence (Gotthelf & Kulkarni 1997).

A new X-ray transient was discovered by *INTEGRAL* on 2013 March 28, from a position consistent with M28, and named IGR J18245–2452 (Eckert et al. 2013). Using *Swift*-XRT observations, Heinke et al. (2013) confirmed the association of the new transient with the core of M28. Romano et al. (2013) and Barthelmy et al. (2013) reported analyses of the X-ray light curve and spectrum of IGR J18245–2452 near the outburst peak, which triggered the *Swift*-BAT on three occasions (Romano et al. 2013). A type I (thermonuclear) X-ray burst from IGR J18245–2452 was detected with the *Swift*-XRT on 2013 April 07 (Papitto et al. 2013a; Linares 2013), identifying the source

as a NS-LMXB. Pavan et al. (2013) reported the radio detection and sub-arcsecond position of IGR J18245–2452 in outburst, on 2013 April 05, which is consistent with only one source from Becker et al. (2003): S23. Using the improved radio location a variable likely optical counterpart to IGR J18245–2452 was found in archival *HST* observations (Pallanca et al. 2013; Cohn et al. 2013). A *Chandra* observation taken on 2013 April 28 (Homan & Pooley 2013) showed no new bright sources in the core of M28, and S23 at a luminosity higher than that measured in 2002.

Papitto et al. (2013b) discovered 254 Hz X-ray pulsations during two *XMM* observations taken on 2013 Apr. 3 & 13, and identified the new transient NS-LMXB with a previously known MRP in an 11 hr orbit: PSR J1824–2452I (Begin 2006). MRPs (Backer et al. 1982) have long been thought to be the evolutionary end point of NS-LMXBs (Alpar et al. 1982). The discovery of accretion-powered millisecond pulsars (AMPs; Wijnands & van der Klis 1998) provided strong evidence for such evolutionary link. While other indirect evidence has been presented (Burderi et al. 2003; Archibald et al. 2009), Papitto et al. (2013b) found IGR J18245–2452 to be the first system directly observed to switch between MRP and AMP phases at different times. IGR J18245–2452 was detected again as an MRP after the 2013 outburst (Papitto et al. 2013c). Burst oscillations were found in the April 07 burst observed by *Swift*, at the 254 Hz spin frequency (Patruno 2013; Papitto et al. 2013b; Riggio et al. 2013).

We present a detailed analysis of the 2013 March–April outburst of IGR J18245–2452 as observed by *Swift*, as well as the thermonuclear burst that led to its NS-LMXB classification (Sec. 3.1). We also study the quiescent properties of IGR J18245–2452, using deep *Chandra* observations of M28, and we find that it features a hard, purely non-thermal and highly-variable quiescent spectrum. We find evidence for a spectral transition around $L_X/L_{Edd} \sim 10^{-4}$ (Sec. 3.2), and a striking variability pattern in the longest *Chandra* observations of IGR J18245–2452 in quiescence (Sec. 3.3). We discuss our results in Section 4, in the context of low-luminosity accretion flows, quiescent emission from NS-LMXBs and X-ray emission from MRPs.

2 DATA ANALYSIS

We give in this Section a detailed explanation of the data reduction and analysis procedures. All luminosities, radiated energies and radii in this work use 5.5 kpc, the distance reported by Harris (1996, 2010 revision) based on HST photometry of M28/NGC 6626 (Testa et al. 2001). When normalizing luminosities to the Eddington limit, we use $L_{Edd} = 2.5 \times 10^{38}$ erg s $^{-1}$. Unless otherwise noted, uncertainties are quoted at the 1σ confidence level and fluxes and luminosities are given in the 0.5–10 keV band. Since hard states emit a sizeable fraction of their total luminosity outside the 0.5–10 keV band covered by the *Swift*-XRT, a bolometric correction ($f_{bol} = 3$) is applied when estimating mass accretion rates (see, e.g., in't Zand, Jonker & Markwardt 2007).

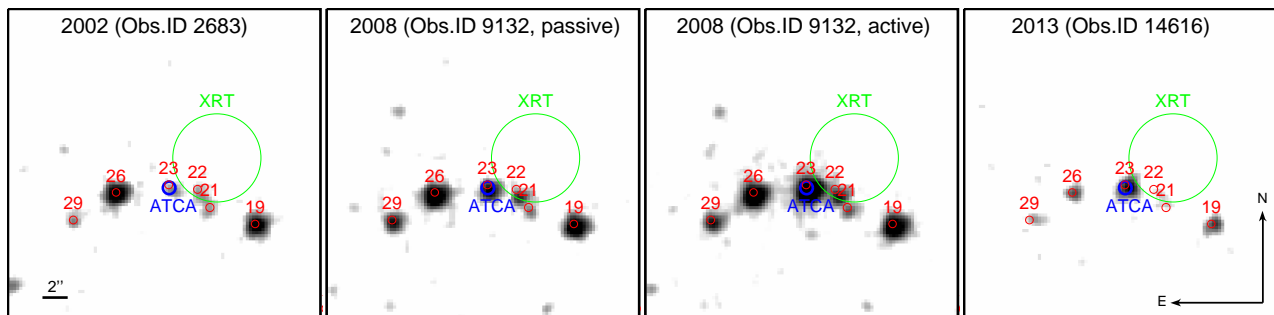


Figure 1. *Chandra*-ACIS-S archival observations of the central parts of M28 in four epochs (from left to right): 2002, 2008 during the passive state, 2008 during the active state and 2013 after the outburst of IGR J18245–2452 (see text for details). Image comparison showing the sources from Becker et al. (2003, red circles), the *Swift*-XRT (Romano et al. 2013, green circle) and ATCA (Pavan et al. 2013, blue circle) locations of the 2013 outburst from IGR J18245–2452. Only source 23 from Becker et al. (2003, S23), marginally consistent with the *Swift*-XRT location (90% c.l. uncertainty of $3.5''$), lies inside the ATCA (90% c.l.) $0.5''$ error circle (which is also consistent with the *Chandra*-HRC position reported by Papitto et al. 2013b).

2.1 Swift

We analysed all *Swift*-XRT observations of M28 available in August 2013, totalling 28 observations and about 37 ksec of on-source time, including pre-planned (target numbers 90442, 32785, 32787) and triggered (triggers 2336, 2369, 2370) observations. All products were extracted using FTOOLS (v. 6.12). The only *Swift* observation taken before the discovery outburst of IGR J18245–2452 (on 2010-06-24) shows a blend of very faint unresolved sources in the core of M28 (Becker et al. 2003, see below), and was not included in the rest of the analysis.

One persistent and one background spectrum were extracted per observation (after running *xrtpipeline*, v. 0.12.6) using pointed data in windowed timing (WT) or photon counting (PC) mode (taking the longest exposure when both modes were present in the same observation). A circular extraction region with a 30-pixel radius centered on the source position (Romano et al. 2013) was used for most observations; an annular region with 5- and 40-pixel radii was used in the brightest PC mode observations in order to correct for pile-up. The X-ray burst was excluded to obtain the persistent spectrum of the corresponding observation. We created ancillary response files using *xrtmkarf* (v. 0.6.0) and an exposure map for each event file using *xrtepomap* (v. 0.2.7), thereby correcting for vignetting and the XRT’s point spread function (PSF). After grouping the spectra to a minimum of 15 counts per bin, we fitted them in the 0.5–10 keV band within *Xspec* (v. 12.7.1; Arnaud 1996) using the latest response matrices from the calibration database (0to12s6_20070901v011 and 0to2s6_20070901v012 for PC and WT mode, respectively) and a simple absorbed power law model.

Swift-XRT cannot resolve the numerous faint ($L_X \lesssim 10^{33}$ erg s $^{-1}$) X-ray sources often present in the center of globular clusters. In the case of M28, twelve sources have been detected with *Chandra* within the $0.24'$ core radius (Becker et al. 2003), which is similar to *Swift*-XRT’s half-power diameter, $0.3'$. The standard background subtraction method, which uses a source free region outside the globular cluster’s core, does not take into account the contribution from nearby faint X-ray sources in the center of M28, which we refer to as “unresolved faint-source background”

(UFB). We investigated whether or not this additional background component affects the flux and spectral parameters from IGR J18245–2452 measured with the XRT, as follows. We extracted a spectrum from the 2002 and 2008 *Chandra*-ACIS observations of M28 (Sec. 2.2) using the same ($\sim 1.2'$ radius) region used for *Swift*-XRT extraction but excluding our source of interest, IGR J18245–2452. The resulting UFB spectrum does not change between the 2002 and 2008 observations and can be fitted with an absorbed power law model with photon index 1.96 ± 0.06 (90% c.l.; $N_H = 2 \times 10^{21}$ cm $^{-2}$), which yields a 0.5–10 keV luminosity of $\sim 4.5 \times 10^{33}$ erg s $^{-1}$ and an XRT count rate of $\sim 1.8 \times 10^{-2}$ c s $^{-1}$.

We then repeated the XRT spectral fits of the persistent emission, adding a second power-law component to the model with parameters frozen at the values found for the UFB spectrum (and a multiplicative constant fixed at 0.926 to take into account the absolute flux calibration difference between ACIS-S3 and the XRT, Tsujimoto et al. 2011). Thus the final model used was $\text{phabs} * (\text{powerlaw} + \text{constant} * \text{powerlaw})$, where the second term is kept fixed and accounts for the UFB. We thereby fit only excess emission above the UFB, i.e., from our source of interest (the only known variable source within the extraction region).

For luminosities above 10^{34} erg s $^{-1}$ we find spectral parameters fully consistent with those found with the standard background subtraction method. When IGR J18245–2452’s luminosity drops below 10^{34} erg s $^{-1}$, however, its flux becomes comparable to that of the UFB and its spectrum cannot be well constrained with *Swift*-XRT. We therefore excluded those observations taken between Apr 19 and May 06, when IGR J18245–2452 was too faint to be disentangled from the UFB. We also fitted together three observations taken on consecutive days (Apr 15–17) in order to improve the spectral constraints on IGR J18245–2452 at the faintest luminosities accessible to *Swift* ($\sim 4 \times 10^{34}$ erg s $^{-1}$). Finally, we verified that fixing N_H to the values found with *Chandra* yields consistent results ($N_H \equiv 2.6 \times 10^{21}$ cm $^{-2}$ gives photon indices lower by 10%, and a similar softening with decreasing L_X , although the fits with this model are worse than those using our preferred free N_H model; Sec. 3).

For the burst time-resolved spectroscopy, we extracted contiguous spectra in 2s steps (4s in the last stages of the

Table 1. Observations and best-fit parameters for the *Chandra*-ACIS spectra of IGR J18245–2452 in quiescence.

Epoch	Observation IDs	Date (dd/m)	Exp. (ksec)	Luminosity ^a (erg s ⁻¹)	Flux ^a (erg s ⁻¹ cm ⁻²)	Γ^b	N_H^c (10 ²¹ cm ⁻²)	χ^2/dof
2002	268-4,5,3	04/7,04/8,11/9	41	$[2.5\pm 0.8]\times 10^{32}$	$[6.6\pm 2.0]\times 10^{-14}$	0.8 ± 0.3	$\equiv 2.6$	4.0/3
2002 ^d	268-4,5,3	04/7,04/8,11/9	41	$[2.2\pm 0.4]\times 10^{32}$	$[5.4\pm 1.0]\times 10^{-14}$	1.2 ± 0.2	$\equiv 2.6$	294.2/647
2008	9132(Average)	07/8	144	$[3.0\pm 0.1]\times 10^{33}$	$[7.2\pm 0.3]\times 10^{-13}$	1.44 ± 0.05	2.6 ± 0.2	257.3/249
2008-A	9132(Active)	07/8	97	$[3.9\pm 0.1]\times 10^{33}$	$[9.2\pm 0.4]\times 10^{-13}$	1.51 ± 0.04	2.9 ± 0.2	33.3/27
2008-P	9132(Passive)	07/8	47	$[5.6\pm 1.0]\times 10^{32}$	$[1.3\pm 0.2]\times 10^{-13}$	1.45 ± 0.15	2.6 ± 0.8	29.7/29
2013	14616	28/4	15	$[3.8\pm 0.7]\times 10^{33}$	$[8.9\pm 1.6]\times 10^{-13}$	1.6 ± 0.2	$\equiv 2.6$	9.5/15

^a Luminosity in the 0.5–10 keV band. Flux in the 0.5–10 keV band, absorbed/observed.

^b Power law photon index (photon flux $\propto E^{-\Gamma}$).

^c Absorbing column density; frozen values are noted with a “ \equiv ” symbol.

^d Fit to the same 2002 spectrum using Cash’s C-statistic.

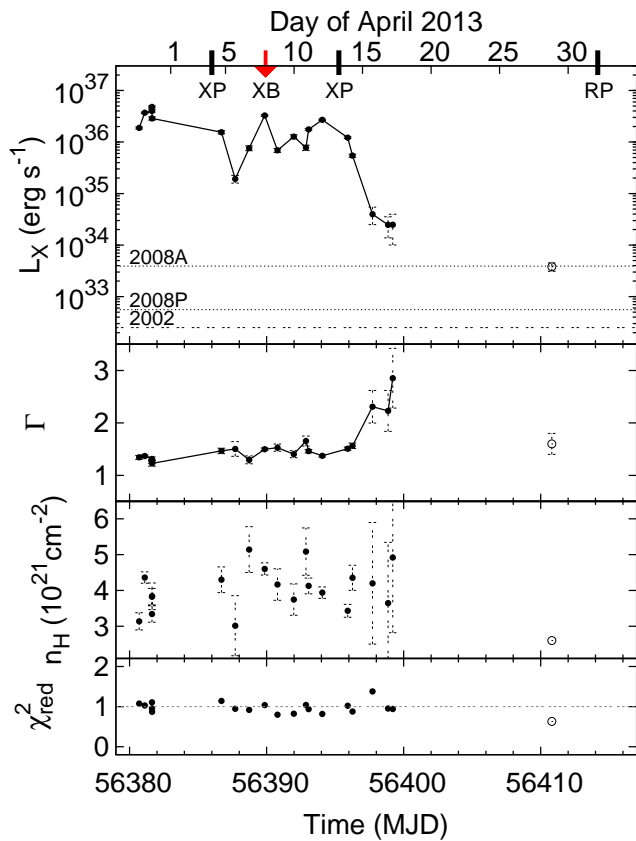


Figure 2. Luminosity (0.5–10 keV) and spectral evolution measured by *Swift* during the 2013 April outburst of IGR J18245–2452. Thick lines across the top axis mark the times of the thermonuclear burst (red arrow labelled “XB”; Fig. 3), the two detections of millisecond X-ray pulsations reported by Papitto et al. (2013b, XP) and the first detection of radio pulsations after the outburst found by Papitto et al. (2013c, RP). Open circles show data from our *Chandra* observation and horizontal lines on the top panel show our quiescent luminosity measurements from previous *Chandra* observations, as indicated (Table 1).

burst tail) and used a ~ 100 s-long interval as background, therefore assuming that the persistent emission remains constant during the burst. As the burst peak count rate was higher than 300 c/s, above the nominal pile-up limit for WT mode, we used an annular extraction region with radii of 1 and 20 pixels centered on the XRT position (Romano et al. 2013). We fitted the resulting spectra as above, but using this time an absorbed black body model with N_H fixed at 4.4×10^{21} cm⁻², the value reported from XRT spectroscopy of IGR J18245–2452’s persistent emission (Romano et al. 2013; Heinke et al. 2013, we also checked that leaving N_H free gives consistent results).

2.2 Chandra

We analysed all publicly available *Chandra*-ACIS-S observations of M28, totalling 41 ksec in 2002 (July–August; obs. IDs 2684, 2685 and 2683; see Becker et al. 2003) and 199 ksec in 2008 (August; obs. IDs 9132 and 9133; see Bogdanov et al. 2011b). Following the discovery of the new transient IGR J18245–2452 (Eckert et al. 2013, Sec. 1), we obtained a 15 ksec *Chandra* ToO observation of M28 on 2013-04-28 (obs. ID 14616, Homan & Pooley 2013), which we also analyse herein. Table 1 shows a summary of the *Chandra*-ACIS observations and spectra. We also analysed the two publicly available *Chandra*-HRC-S observations of M28, taken in 2002 (November, obs. 2797) and 2006 (May, obs. 6769). Even though no spectral information is available in the HRC data, we extracted background-corrected count rates from IGR J18245–2452 using a 1.6”-radius circular region, in order to constrain the source quiescent luminosity at all possible times. All products were extracted using tools and scripts from the latest available CIAO¹ package (v. 4.5; Fruscione et al. 2006).

Figure 1 shows four smoothed *Chandra*-ACIS-S images of M28’s core taken in 2002, 2008 during the passive state, 2008 during the active state and 2013 after the outburst of IGR J18245–2452 (see Table 1 for observation IDs and exposure times). See Sections 3.3 and 4.3, respectively, for a definition and discussion of active/passive

¹ Chandra Interactive Analysis of Observations, available at <http://cxc.harvard.edu/ciao/>

states. Superposed are the initial *Swift*-XRT location of IGR J18245–2452 (Romano et al. 2013, green circle), the position of the ATCA radio counterpart found during its 2013 outburst (Pavan et al. 2013, blue circle) and the nearby faint X-ray sources studied by Becker et al. (2003, red circles). Only source 23 from Becker et al. (2003) is consistent with the ATCA position (as noted by Pavan et al. 2013; Papitto et al. 2013b), which is also consistent with the *Chandra*-HRC location reported by Papitto et al. (2013b), and marginally consistent with the *Swift*-XRT location (Romano et al. 2013, which was not “enhanced” with UVOT attitude correction). Hence we confirm the association of the new transient source IGR J18245–2452 with source 23 of Becker et al. (2003).

Source spectra were extracted from primary event files using circular regions of 2–4 pixel radii and the script *specextract* (v. 10), which creates the corresponding ancillary response files corrected for *Chandra*’s PSF. We grouped the resulting spectra to a minimum of 15 counts per energy bin, and extracted the background spectrum from a 10-pixel circular source-free region. In order to increase the signal-to-noise ratio (S/N) in the 2002 spectrum of IGR J18245–2452’s quiescent counterpart, we summed the spectra and event files from all three observations using the CIAO scripts *combine_spectra* and *reproject_obs*, respectively.

3 RESULTS

3.1 Outburst evolution and thermonuclear burst

Figure 2 shows an overview of the 2013 outburst from IGR J18245–2452 including the evolution of the luminosity, photon index, and the reported detection dates of the thermonuclear burst (Papitto et al. 2013a; Linares 2013), X-ray pulsations (Papitto et al. 2013b) and reappearance of radio pulsations (Papitto et al. 2013c). A simple absorbed power law model provides a good fit to the persistent (accretion-powered) *Swift*-XRT spectra, and yields photon indices in the range 1.2–2.8. We find a maximum 0.5–10 keV outburst luminosity of $(4.8 \pm 0.2) \times 10^{36}$ erg s⁻¹ ($\sim 6\%$ of L_{Edd} assuming a bolometric correction factor $f_{bol}=3$) on 2013 March 30, and a power law (photon) index of 1.26 ± 0.03 on the same date. These luminosities and photon indices, as well as the burst behaviour (see below) and the presence of millisecond X-ray pulsations (Papitto et al. 2013b), are all consistent with the properties of the so-called atoll sources (a sub-class of low-luminosity NS-LMXBs, Hasinger & van der Klis 1989) in the hard state (Linares 2009).

We present the main properties and spectral evolution of the thermonuclear burst detected with *Swift*-XRT in Table 2 and Figure 3, respectively. The burst spectra are well fitted with a simple absorbed blackbody model and show the unequivocal temperature drop (“cooling tail”) along the flux decay, which is consistent with a simple exponential decay with an e-folding time of 26.6 ± 1.8 s. The count rate light curve shows a ~ 10 s-long plateau near its maximum with a possible double-peak structure, both commonly seen in type I X-ray burst profiles. We do not find spectral evidence of photospheric radius expansion around the burst peak (e.g., Kuulkers et al. 2003), and the bolometric luminosity does not exceed 2×10^{38} erg s⁻¹. The blackbody radii

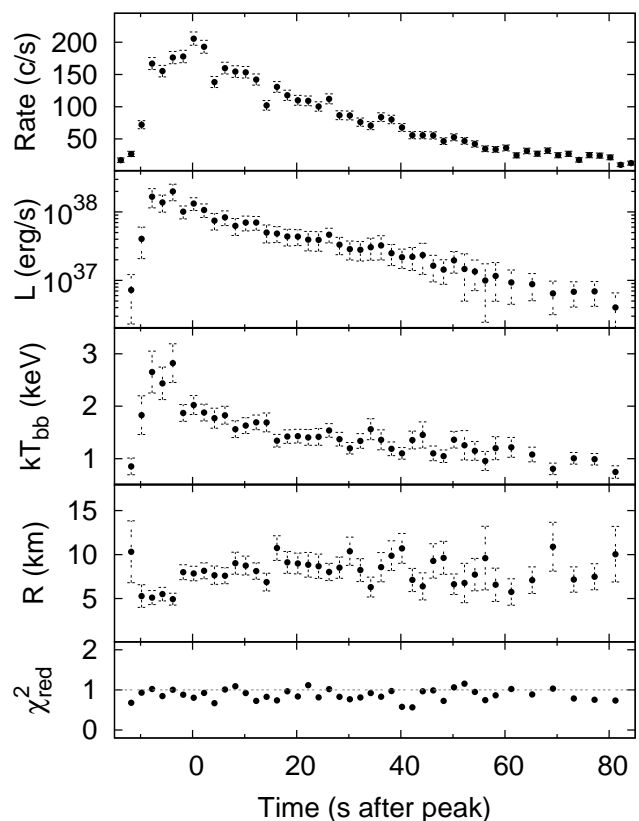


Figure 3. Net count rate (0.5–10 keV), bolometric luminosity and spectral evolution during the type-I (thermonuclear) X-ray burst from IGR J18245–2452 detected by *Swift* on 2013-04-07 (Papitto et al. 2013a; Linares 2013).

Table 2. Properties of the type I X-ray burst from IGR J18245–2452 observed by *Swift* on 2013-04-07.

Peak time (of max. net rate) (UTC)	22:15:42
Rise time (25% to 90% of peak rate) (s)	6.5 ± 1.0
Duration (until 10% of peak rate) (s)	82.5 ± 1.0
Bolometric peak luminosity (10^{38} erg s ⁻¹)	2.0 ± 0.5
Bolometric radiated energy (10^{39} erg)	3.9 ± 0.2
Persistent L_X (0.5–10 keV; 10^{36} erg s ⁻¹)	3.3 ± 0.1

that we measure during the burst (without color/redshift corrections) are in the [5–10] km range, also typical of thermonuclear bursts from NSs.

The burst was detected about 10 d after the beginning of the outburst (Papitto et al. 2013a; Linares 2013), when the luminosity and inferred mass accretion rate (\dot{M}) were a few percent of the Eddington limit ($\sim 4\%$ L_{Edd} from the measured 0.5–10 keV luminosity of 3.3×10^{36} erg s⁻¹ and using $f_{bol}=3$). At this \dot{M} , close to the boundary between the pure He and mixed H/He ignition regimes, H is expected to burn stably and thus He ignition triggers the bursts (Bildsten 1998). The long decay timescale, together with the lack of radius expansion, suggest that the burst ignites in a mix of H and He (e.g., Galloway et al. 2008). The total radiated bolometric burst energy that we measure, 3.9×10^{39} erg,

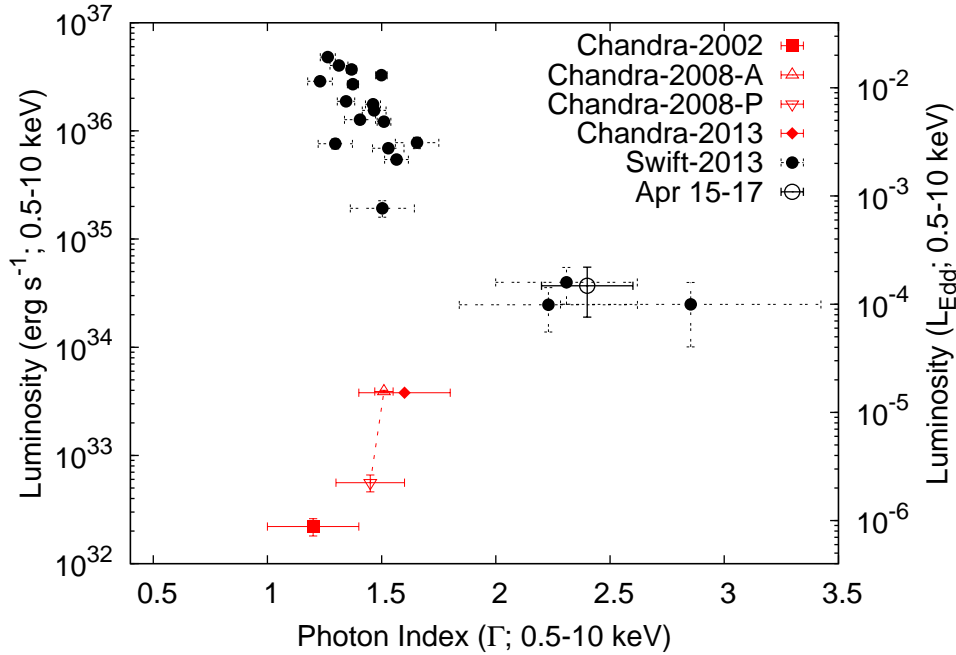


Figure 4. Photon index (Γ) vs. luminosity (L_X) for IGR J18245–2452 from outburst to quiescence, spanning five orders of magnitude in L_X . The $\Gamma - L$ anticorrelation (“softening towards quiescence”) at relatively high L_X ($10^{34} - 10^{37} \text{ erg s}^{-1}$) turns into a positive correlation below $L_X \sim 10^{-4} L_{\text{Edd}}$. The red dotted line connects the 2008 active and passive states (Sec. 3.3; Figs. 5 & 6).

corresponds to an ignition depth of $\sim 9.6 \times 10^7 \text{ g cm}^{-2}$ (assuming solar-abundance homogeneously-distributed fuel releasing 4.4 MeV nucleon $^{-1}$; e.g., Galloway et al. 2008), which can be reached when accreting at 4% of the Eddington rate in only ~ 0.3 d. This crude estimate of the expected burst recurrence time suggests that more thermonuclear bursts occurred during the 2013 ~ 25 d-long outburst, but given that *Swift*-XRT observed IGR J18245–2452 for a total accumulated exposure of ~ 0.4 d, it is not surprising that it only detected one thermonuclear burst.

3.2 Between outburst and quiescence

We find an anticorrelation between the persistent luminosity, L_X , and the photon index, Γ , measured by *Swift* during the outburst peak and decay when L_X/L_{Edd} decreased from 10^{-2} to 10^{-4} . Γ increases from 1.3 above $L_X/L_{\text{Edd}}=10^{-2}$ to ~ 2.5 at $L_X/L_{\text{Edd}}=10^{-4}$. This softening during the decay to quiescence (already noticeable in Fig. 2, top two panels) can be clearly seen in Figure 4, where we plot L_X vs. Γ over five orders of magnitude in L_X (note that special care was taken to avoid background contamination in the *Swift* spectra; Sec. 2.1). In order to test the significance of this anticorrelation, we calculate Spearman’s rank-order coefficient (r) using all (19) values of $[L_X, \Gamma]$ measured with *Swift* and find $r = -0.80$, which deviates from 0 at the 4.1σ confidence level (the same test using only the brightest *Swift*-XRT data at $L_X > 10^{35} \text{ erg s}^{-1}$ gives $r = -0.67$ and a 2.8σ significance). Such softening of the X-ray spectrum from (hard state) outburst to quiescence has been previously seen in both NS and BH transients (Wu & Gu 2008; Armas Padilla et al. 2011; Plotkin, Gallo & Jonker 2013, see discussion in Sec. 4.1).

The absorbing column densities during the 2013 out-

burst ($N_H = [3-5] \times 10^{21} \text{ cm}^{-2}$ at $L_X > 10^{34} \text{ erg s}^{-1}$) are higher than those measured in quiescence by *Chandra* (Sec. 3.3, Table 1). This can be seen from our fits to the *Swift* persistent spectra (Figure 2), which yield an average $N_H = [4.0 \pm 0.1] \times 10^{21} \text{ cm}^{-2}$, higher than the value of $[2.6 \pm 0.2] \times 10^{21} \text{ cm}^{-2}$ measured in the 2008 observations when the luminosity was $L_X = [0.6-4] \times 10^{33} \text{ erg s}^{-1}$. Fixing N_H to the value found with *Swift* during outburst does not yield acceptable spectral fits to the *Chandra* 2008 quiescent spectrum (reduced χ^2 increases from 1.0 to 1.3 for 248 dof). This result suggests that intrinsic changes in the absorbing material take place between outburst and quiescence, perhaps linked to the increased mass accretion rate during outburst, and cautions against the blind use of N_H values measured in outburst for quiescent studies.

3.3 Variable quiescence

All *Chandra* spectra are well fitted with a simple absorbed power law model. We present in Table 1 the results of the spectral fits to the *Chandra*-ACIS quiescent spectra at different epochs, between 2002 and 2013. We show the resulting $L_X - \Gamma$ relation in Figure 4, which covers the $L_X/L_{\text{Edd}} = [10^{-6} - 10^{-4}]$ range, together with the *Swift* data at higher luminosities, $L_X/L_{\text{Edd}} = [10^{-4} - 10^{-2}]$.

Our *Chandra* analysis shows that IGR J18245–2452 is a hard, purely non-thermal X-ray source in quiescence, with a 0.5–10 keV luminosity that varies by more than one order of magnitude, $2.5 \times 10^{32} \text{ erg s}^{-1}$ in 2002 and up to $3.8 \times 10^{33} \text{ erg s}^{-1}$ in 2008, while the photon index Γ remained between 1 and 1.5. Soon after its 2013 outburst, during a *Chandra* observation taken on 2013-04-28 (Homan & Pooley 2013), we detected IGR J18245–2452 with the same luminos-

ity (3.9×10^{33} erg s $^{-1}$) and spectral index ($\Gamma \simeq 1.5$) as those measured in 2008 (during its active state, see below).

We show in Figure 5 a comparison between the unfolded quiescent spectra from IGR J18245–2452 at different epochs, to illustrate the large luminosity changes that take place with little or no change in the spectral shape. Given that all the spectra taken at luminosities below 10^{34} erg s $^{-1}$ ($L_X/L_{Edd} < 10^{-4}$), are harder than those measured by *Swift* in the latest stages of the outburst decay, we define quiescence as $L_X/L_{Edd} < 10^{-4}$ (Figure 4). With this definition, and extrapolating the latest flux decay seen by *Swift*, we estimate that the outburst finished around 2013-04-22 (with an uncertainty of about 4 d) and lasted for 25 d, which implies that both 2013 *Chandra* observations (Homan & Pooley 2013; Papitto et al. 2013b) were taken when IGR J18245–2452 was in quiescence.

The most stringent limits on the thermal NS component come from the observations where IGR J18245–2452 is the faintest, taken in 2002. We extracted a spectrum from IGR J18245–2452 from the three 2002 ACIS-S observations combined (Sec. 2.2). The spectrum is well fitted with a simple absorbed power-law model, which yields a 0.5–10 keV luminosity of $[2.5 \pm 0.8] \times 10^{32}$ erg s $^{-1}$ (Table 1). In order to get upper limits on the NS temperature and luminosity in quiescence, we added a NS atmosphere component to the spectral model (NSATMOS, Heinke et al. 2006, assuming a 1.4 M_\odot , 10 km NS with normalization fixed at 1 and a distance of 5.5 kpc). We then fitted the spectrum using chi-squared statistics (binning to 15 counts/bin, which left us with 6 bins) and using unbinned data and the C-statistic. We obtain consistent constraints from the two methods. We find upper limits (at 90% confidence) on the 0.1–10 keV (gravitationally redshifted) thermal quiescent luminosity $L_{NS}^\infty < 7 \times 10^{31}$ erg s $^{-1}$ and on the corresponding (intrinsic, redshift-corrected) NS surface effective temperature $T_{eff} < 6.6 \times 10^5$ K.

The two public *Chandra* HRC-S observations (Sec. 2.2) show IGR J18245–2452 at slightly fainter levels than the 2002 ACIS observations. We find net source count rates of $(7.5 \pm 0.9) \times 10^{-4}$ c s $^{-1}$ and $(7.1 \pm 1.0) \times 10^{-4}$ c s $^{-1}$ in the November 2002 and May 2006 observations, respectively. Although these data provide no spectral information, we can estimate the quiescent luminosity assuming that the spectral shape is similar to that measured in the *Chandra*-ACIS observations. For $N_H = 2.6 \times 10^{21}$ cm $^{-2}$ and Γ in the range 1.0–1.5 we obtain $L_X = [1.1\text{--}2.1] \times 10^{32}$ erg s $^{-1}$ during the 2002 and 2006 HRC observations.

Interestingly, comparing our *Chandra* and *Swift* results shows that the spectrum does not continue to soften at luminosities $L_X/L_{Edd} < 10^{-4}$, but it hardens instead (Fig. 4). All four *Chandra* spectra (taken in 2002, 2008 and 2013) are consistent with $\Gamma \simeq 1.5$ (a fit to a constant Γ gives $\chi^2 = 2.7$ for 3 d.o.f. and a Spearman rank test yields no significant correlation, although the sample is obviously small and fractional errors on Γ are large). However, including the three lowest- L_X *Swift* measurements (at $L_X/L_{Edd} \sim 10^{-4}$) yields $r = 0.93$ and a positive correlation with a 3σ significance. This strongly suggests that the X-ray spectrum hardens while reaching deep quiescence ($L_X/L_{Edd} = 10^{-4} \rightarrow 10^{-6}$), after softening in the hard state during the outburst decay ($L_X/L_{Edd} = 10^{-2} \rightarrow 10^{-4}$, see Sec. 3.2). More frequent and sensitive observations of the decay to quiescence may allow

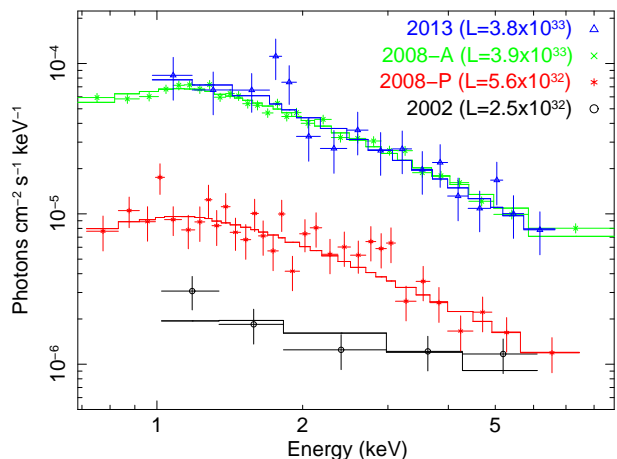


Figure 5. Quiescent *Chandra*-ACIS-S unfolded spectra from IGR J18245–2452 (S23) at different epochs, as noted (A and P stand for active and passive states within quiescence in 2008, see text). The 0.5–10 keV luminosity in erg s $^{-1}$, which varies by more than one order of magnitude, is indicated between parenthesis.

a better measurement of this spectral transition between outburst and quiescence. We tentatively place the luminosity at which this transition occurs at $L_X/L_{Edd} \sim 10^{-4}$ (see Figure 4).

The 2008 quiescent *Chandra*-ACIS light curves show striking variability on several time scales (see Figure 6). We find two clearly distinguishable states or “modes” in the light curve, at two distinct average count rates, and rapid changes between them (within less than 500 s). We identify a low luminosity *passive state* and a high luminosity *active state* during quiescence, below and above a *Chandra*-ACIS 0.5–8 keV count rate of 0.03 c s $^{-1}$, respectively (dashed purple line in Figure 6). These are most clearly visible in the 144 ksec-long observation taken on 2008-08-07 (observation 9132; Fig. 6, left), but also three days later in the 55 ksec-long observation taken on 2008-08-10 (observation 9133; Fig. 6, right). Even though it was taken when L_X was similar to the 2008 active state (Table 1), the 2013 *Chandra* light curve does not show rapid intensity changes. However, we cannot rule out the presence of mode switching during that observation, as the exposure time was shorter (15 ksec) and the count rate was lower ($1.2 \pm 0.4 \times 10^{-2}$ c s $^{-1}$) than those in the 2008 observation.

After ~ 9 ksec in the active state since the beginning of observation 9132, the source switched to the passive state for about 3 ksec and after a short (~ 2.5 ksec) re-flare to the active state, it stayed in the passive state for another ~ 35 ksec (Fig. 6, top). Then IGR J18245–2452 switched back to the active state for ~ 85 ksec, with a few short (~ 1 ksec) drops in count rate suggestive of short excursions to the passive state. For the last ~ 9.5 ksec the source stayed in the passive state. Three days later, observation 9133 starts with a ~ 2.5 ksec flare to the active state, then after 38 ksec of passive state with two more short (about 2 and 4 ksec-long) flares the source switches back to the active state for about 27 ksec, and switches back to the passive state at the end of the observation. We also find rapid (~ 500 – 1000 s) and less

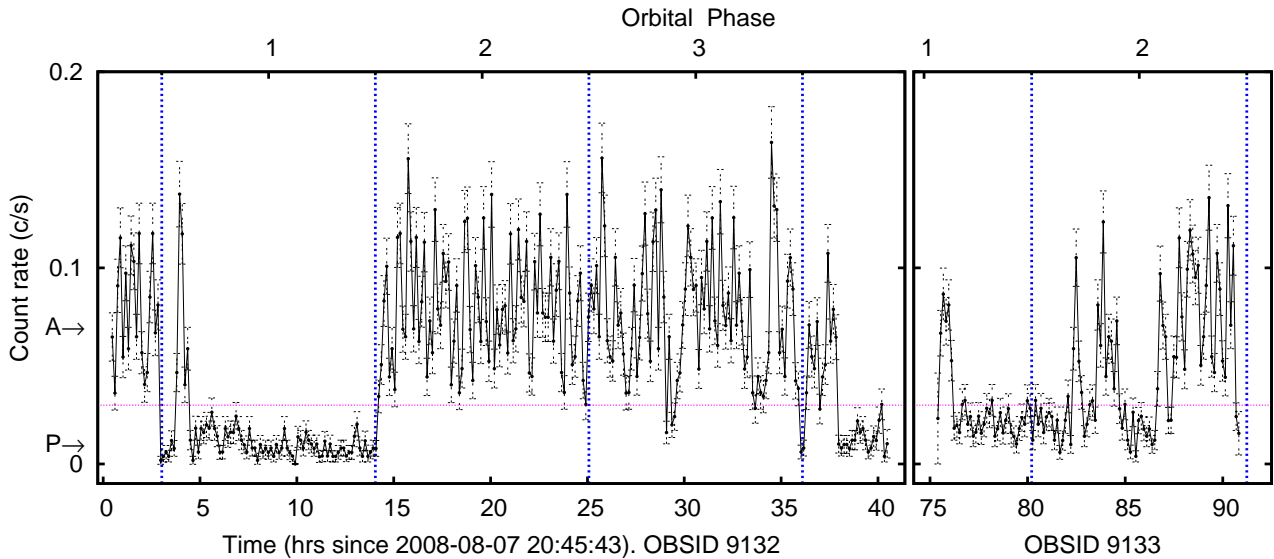


Figure 6. Quiescent light curve (500 s bins, background-subtracted) from IGR J18245–2452 (S23), measured with *Chandra*-ACIS in 2008 August 7 (left) and 10 (right). The source switches between active (A) and passive (P) states (defined by the horizontal purple line), with a factor ~ 7 change in luminosity and no detectable spectral change (Sec. 3.3). Vertical blue lines mark orbital phase 0.5 (from the ephemerids given by Papitto et al. 2013b).

pronounced (factor ~ 2 – 3 changes in count rate) variability in the light curves of both the active and passive states.

The hardness ratio (defined as the ratio of counts in the 2–8 keV and 0.5–2 keV bands, and calculated in 2 ksec bins) is consistent with being constant during both 2008 observations. We extracted spectra of the active and passive states, using the above definition and the same procedures explained in Sec. 2.2. Both are well-fit with an absorbed power-law model, and the best-fit Γ and N_H in the active and passive states are fully consistent (see Table 1). In order to search for small spectral variations, we repeated the fits to the active and passive state spectra keeping N_H linked or fixed to its average value, and again found Γ values consistent within the reduced (1–5%) fractional errors. We measure a 0.5–10 keV luminosity of 3.9×10^{33} erg s $^{-1}$ and 5.6×10^{32} erg s $^{-1}$ for the active and passive state, respectively. Thus when the source switches between active and passive quiescent states the luminosity changes by a factor of ~ 7 with no detectable change in the spectrum. Figure 5 shows the active and passive state spectra, as well as the other quiescent spectra of IGR J18245–2452 measured with *Chandra* in 2002 and 2013.

It is perhaps worth noting that the first passive state begins and ends at orbital phase 0.5 (first two vertical lines in Fig. 6, from orbital ephemerids reported by Papitto et al. 2013b), i.e., when the NS is at the descending node (approaching most rapidly). Even though one of the short dips later in that observation also occurs at orbital phase 0.5, the variability pattern does not recur and in general the source switches between active and passive states at different orbital phases.

4 DISCUSSION

4.1 Underluminous accretion flows and softening to quiescence

We found that when IGR J18245–2452’s luminosity decayed from $L_X/L_{Edd} \sim 10^{-2}$ to $L_X/L_{Edd} \sim 10^{-4}$ the *Swift*-XRT (0.5–10 keV) spectrum could be described by a simple power-law, and the photon index Γ increased from 1.3 at the highest luminosities to ~ 2.5 at the lowest luminosities (Section 3.2). Similar softening has been seen before in other systems, both NS (Armas Padilla et al. 2011; Degenaar, Wijnands & Miller 2013) and BH (Wu & Gu 2008; Sobolewska et al. 2011; Plotkin, Gallo & Jonker 2013) transients, and it appears to be a general observable of LMXBs in the hard state when they transit to quiescence. In the context of advection dominated (radiatively inefficient) accretion flows (ADAFs; Narayan & Yi 1995), this behavior can be explained by a change in the optical depth for Compton up-scattering: as \dot{M} decreases, the optical depth of the ADAF and the fraction of hard/up-scattered photons decrease, causing a softening of the X-ray spectrum (Esin, McClintock & Narayan 1997, predict a change in Γ of $1.5 \rightarrow 2.2$ due to this effect). Other physical jet-based interpretations for this softening towards quiescence exist, which assume that X-ray emission from the jet dominates in quiescence (see, e.g., discussion in Sec. 4.2 of Plotkin, Gallo & Jonker 2013, and references therein).

In the case of accreting NSs the interpretation of the observed X-ray spectra at low luminosities should also consider potential thermal surface emission, coming from either low-level accretion onto the NS or from the crust heated up during outburst. Indeed, a thermal component has been found in X-ray spectra of NS-LMXBs at a luminosity of a few times 10^{34} erg s $^{-1}$, in both transient (Degenaar, Wijnands & Miller 2013) and persistent accretors (Armas Padilla, Degenaar & Wijnands 2013). It is un-

clear at which luminosity and in which systems this component becomes important, and therefore we cannot assess whether or not it contributes to the softening of NS-LMXBs when they decay from $L_X/L_{Edd} \sim 10^{-2}$ to $L_X/L_{Edd} \sim 10^{-4}$. The lowest luminosity *Swift*-XRT spectra of IGR J18245–2452, at $L_X \simeq 4 \times 10^{34}$ erg s $^{-1}$, do not show evidence of a thermal component and allow only weak constraints on the presence of such component. We derive a 90% upper limit on the thermal fraction of <24% (defined as the fractional contribution of a blackbody component to the 0.5–10 keV luminosity). This upper limit is derived assuming a temperature of 0.3 keV, like that measured by Armas Padilla, Degenaar & Wijnands (2013) at similar L_X , and is compatible with the range of values found by the same authors in other NS-LMXBs (8–53%).

The deep *Chandra* observations allow us to place stringent constraints on the presence of a thermal component at lower luminosities, which correspond to a thermal fraction lower than 3% at $L_X \simeq 2.5 \times 10^{32}$ erg s $^{-1}$ (Secs. 3.3 & 4.2). We thus conclude that if an undetected thermal component is responsible for the spectral softening in the decay to quiescence observed with *Swift* (Sec. 3.2), then this component should virtually disappear when the luminosity drops below $\sim 10^{34}$ erg s $^{-1}$. This in turn suggests that such thermal component would be accretion-powered rather than crustal-heat-powered, and that the accretion flow is able to reach the NS surface and produce thermal emission down to $L_X/L_{Edd} \sim 10^{-4}$ (see also Armas Padilla, Degenaar & Wijnands 2013). We note, however, that for dipole magnetic fields of 10^8 G accretion onto the NS surface at such low luminosities may be halted by the propeller mechanism (Illarionov & Sunyaev 1975; Campana et al. 1998).

4.2 Active and non-thermal quiescence

We have shown that in quiescence, which we define as $L_X/L_{Edd} < 10^{-4}$ (Sec. 3.3), the new NS X-ray transient in M28 IGR J18245–2452 is fully dominated by a hard power-law spectral component, with a photon index of 1–1.5. By comparing *Chandra*-ACIS observations of M28 taken years apart (between 2002 and 2013), we have also shown that the quiescent 0.5–10 keV luminosity varies by more than an order of magnitude (between 2.5×10^{32} erg s $^{-1}$ in 2002 and 3.8×10^{33} erg s $^{-1}$ in 2008 and 2013). All these properties resemble the quiescent behavior of the NS X-ray transient EXO 1745–248 in the globular cluster Terzan 5 in great detail (Wijnands et al. 2005; Degenaar & Wijnands 2012). The reason for such large fluctuations in quiescence is not clear (see, e.g., Degenaar & Wijnands 2012, for an in-depth discussion). A possible explanation is that continued low-level accretion is occurring in the system, although if that were to reach the NS surface one would expect detectable thermal emission (e.g., Zampieri et al. 1995; Soria et al. 2011) instead of a purely non-thermal quiescent spectrum.

On the other hand, the similarities between the X-ray emission of some quiescent NS-LMXBs and MRPs (Bogdanov, Grindlay & van den Berg 2005) also apply to IGR J18245–2452. Namely, non-thermal and variable X-ray emission has also been seen in the NS-LMXBs Cen X-4 (Rutledge et al. 2001), Aql X-1 (Campana & Stella 2003),

SAX J1808.4–3658 (Campana et al. 2002) and in the MRPs 47 Tuc W (Bogdanov, Grindlay & van den Berg 2005) and PSR J1023+0038 (Archibald et al. 2010).

We can compare the quiescent X-ray properties of IGR J18245–2452 and PSR J1023+0038 with some more detail, since these are the only two MRPs that have shown evidence for accretion. They share low-luminosity and remarkably hard quiescent spectra, with $L_X \simeq 2.5 \times 10^{32}$ erg s $^{-1}$, $\Gamma \simeq 1.2$ and $L_X \simeq 9.4 \times 10^{31}$ erg s $^{-1}$, $\Gamma \simeq 1.26$ for IGR J18245–2452 and PSR J1023+0038, respectively. Archibald et al. (2010) reported a marginal detection of a thermal component in PSR J1023+0038, contributing with 6% of L_X . Our upper limit on a blackbody component at the lowest L_X (<3%, Sec. 3.3) rules out the presence of a similar component in IGR J18245–2452. The same authors found modulations of the X-ray flux from PSR J1023+0038 at the orbital (4.8 hr) and spin (1.7 ms) periods. The data presented herein do not allow a search for ms X-ray pulsations at low L_X , due to insufficient time resolution. The long-term variability that we find during the 2008 observations is more rich than that found in PSR J1023+0038, and it does not seem to be related with the binary orbit (Secs. 3.3 & 4.3).

No thermal component is detected at the lowest luminosities (Sec. 3.3), corresponding to an upper limit on the bolometric intrinsic thermal luminosity of 1.3×10^{32} erg s $^{-1}$ (for a gravitational redshift of 1.3). We can compare this to estimates of the incandescent thermal emission produced by deep crustal heating (Haensel & Zdunik 1990, 2008; Brown, Bildsten & Rutledge 1998; Degenaar, Wijnands & Miller 2013), which should yield a luminosity $\simeq \langle \dot{M} \rangle Q/m$, where we take $Q \simeq 2$ MeV as the total heat deposited per accreted nucleon, $\langle \dot{M} \rangle$ is the long-term average mass accretion rate onto the NS, and m the atomic mass unit. We estimate an average $\dot{M} \sim 2 \times 10^{16}$ g s $^{-1}$ in the 2013 outburst from our measured *Swift*-XRT luminosities (Sec. 3.1; using $f_{bol}=3$ and assuming accretion onto a $1.4M_\odot$ -mass 10 km-radius NS). For a 25 d outburst duration, this implies an outburst recurrence time longer than ~ 20 yr in order to produce a luminosity lower than our upper limit. Alternatively, enhanced neutrino cooling may be acting to reduce the NS core temperature in IGR J18245–2452 down to the observed levels ($T_{eff} < 6.6 \times 10^5$ K, Sec. 3.3), as reported in other NS transients (see, e.g., Heinke et al. 2007; Wijnands, Degenaar & Page 2013). Given that IGR J18245–2452 is active as a rotation-powered pulsar when it is not accreting (as the MRP PSR J1824–2452I; Papitto et al. 2013b), we can compare the upper limit on its thermal luminosity with the typical thermal emission from other MRPs. According to most pulsar models, the polar caps can be heated up by relativistic particles generated when the radio pulsar is on, producing thermal pulsed X-ray emission (e.g., Zavlin 2007). Thermal luminosities measured in MRPs are typically in the range 10^{30} – 10^{31} erg s $^{-1}$, which is compatible with our upper limit of 7×10^{31} erg s $^{-1}$.

When the non-thermal power-law spectral component in quiescent NS-LMXBs is detected and well constrained, the photon index is similarly low, between 1 and 1.5 (we note that the error bars are relatively large). Our results for IGR J18245–2452 are consistent with these typical NS values, which seem to show harder quiescent spectra than black hole (BH) systems, most of which have a photon index of ~ 2 in quiescence (Corbel, Tomsick & Kaaret 2006;

Plotkin, Gallo & Jonker 2013). Thus, while we find evidence for a spectral hardening below $L_X/L_{Edd} \sim 10^{-4}$ (with the photon index Γ reaching 1–1.5; Sec. 3.3), in BH transients Γ seems to saturate below $L_X/L_{Edd} \sim 10^{-5}$ at a value close to 2 (Plotkin, Gallo & Jonker 2013). This suggests that different processes cause the quiescent power-law component in NS and BH X-ray binaries. For BHs this emission is likely due to some form of radiatively inefficient accretion flow but it is possible that in the case of NSs another process is at work. Two emission mechanisms have been proposed for the non-thermal X-rays from NS-LMXBs in quiescence, in order of increasing luminosity: i) an *intrabinary shock* between the pulsar wind and the flow of mass transferred/outflowing from the companion star (originally proposed for MRPs, Arons & Tavani 1993; Campana et al. 1998); and ii) accretion onto the NS magnetosphere, or *magnetospheric accretion* (Campana et al. 1998).

4.3 At the boundary between accretion- and rotation-powered X-rays?

We found striking variability in the 2008 *Chandra* observations of IGR J18245–2452 (Sec. 3.3): sharp transitions between two distinct (active and passive) modes, namely, recurrent, large (factor 7) and rapid ($\lesssim 500$ s) changes in L_X , in the $[0.6\text{--}3.9] \times 10^{33}$ erg s $^{-1}$ range. The detected emission was purely non-thermal and the spectra of the active and passive states were consistent within the errors (photon index $\simeq 1.5$ and no detectable change in absorption; Table 1). Campana, Stella & Kennea (2008) found that the AMP SAX J1808.4–3658 seems to switch between two states when approaching quiescence. Those states were apparent only in the long-term (100 d long) *Swift* light curve, they showed clear spectral variability and a smaller change in luminosity ($L_X = [1.5\text{--}5] \times 10^{32}$ erg s $^{-1}$ and $\Gamma = [1.7\text{--}2.7]$). It seems therefore unlikely that they have the same origin as the active and passive states that we report herein. The mode switching that we observe in IGR J18245–2452, on the other hand, might be reminiscent of the correlated X-ray/radio mode switches recently found by Hermsen et al. (2013) in the old isolated pulsar PSR B0943+10. The latter pulsar is obviously not accreting, and the onset of accretion in IGR J18245–2452, confirmed at least at high X-ray luminosities, suggests that the accretion flow plays a role in the state changes presented in this work, and thus that the physical mechanisms responsible for mode switches in these two pulsars are different.

Three of the transitions coincide with orbital phase 0.5 (NS at descending node) but this is not always the case, and in general mode switching occurs at different orbital phases. Changes in absorption due to matter in different regions of the binary system crossing the line of sight would leave an imprint in the spectrum which we do not observe, and hence cannot explain the mode changes. Intrabinary shock emission is expected (Arons & Tavani 1993) and possibly observed in MRPs (Stappers et al. 2003; Bogdanov, Grindlay & van den Berg 2005) to be modulated at the orbital period. Mildly relativistic speeds in the shocked region can lead to Doppler boosted emission and to orbital modulation of the measured non-thermal X-rays. In the case of IGR J18245–2452, however, the large amplitude and aperiodic nature of the observed variability do not sup-

port a scenario where the mode switching is due to Doppler boosting in the line of sight changing along the orbit.

The available data thus suggest that stochastic changes between two different non-thermal emission processes (which produce very similar spectra) are taking place. One possible explanation is that the observed variability reflects rapid transitions between magnetospheric accretion at high luminosities (3.9×10^{33} erg s $^{-1}$) and intrabinary shock emission at low luminosities (5.6×10^{32} erg s $^{-1}$). In this scenario, the magnetospheric radius r_m during the 2008 *Chandra* observations would be close to the light cylinder radius ($r_{lc} \simeq 186$ km for the 254 Hz spin frequency; Papitto et al. 2013b), and fluctuations in the mass accretion rate \dot{M} would produce the observed transitions. A small drop in \dot{M} would cause r_m to expand beyond r_{lc} , which would turn on the radio pulsar and create an intrabinary shock responsible for the emission in the passive state. An increase in \dot{M} could bring r_m back inside the light cylinder, turning off the radio pulsar and allowing for magnetospheric accretion to take over in the active state. We stress that this scenario involves a balance between the pulsar wind and the inner accretion flow, likely in the form of a hot optically thin flow given the extremely low L_X , and that an optically thick accretion disk may still be present at much larger radii ($r \gg r_{lc}$) (see, e.g., Wang et al. 2009).

The active and passive states of IGR J18245–2452 correspond to bolometric luminosities (L_{bol}) 1.2×10^{34} erg s $^{-1}$ and 1.7×10^{33} erg s $^{-1}$, respectively (using again $f_{bol} = 3$; Sec. 2). Assuming a typical neutron star mass of $1.4 M_\odot$ and radius of 10 km, the magnetospheric radius r_m for spherically symmetric accretion can be expressed as (Lamb, Pethick & Pines 1973; Patruno et al. 2009):

$$r_m = 7.8 \left[\frac{B}{10^8 \text{ G}} \right]^{4/7} \left[\frac{L_{bol}}{L_{Edd}} \right]^{-2/7} \text{ km} \quad (1)$$

Thus for a value of the magnetic field of $B \sim 10^8$ G (typical of all AMPs with a measured B field; see, e.g., Table 4 in Patruno & Watts 2012), the magnetospheric radius r_m will move from about 130 km during the active state up to about 230 km during the passive state. Given that the light cylinder radius $r_{lc} \simeq 186$ km, the magnetosphere will become devoid of material up to the light cylinder as the accretion rate drops from the active to the passive state. This in turn might activate the radio pulsar mechanism and turn on the radio pulsar during the passive states. A higher value of the B field, above 10^9 G, would instead give $r_m > r_{lc}$ for the observed luminosities during the active state. This therefore suggests that, if this interpretation of the active/passive states is correct, the B field of IGR J18245–2452 is similar to that of other AMPs.

A clear prediction of this simple picture is that the radio pulsar should be on during the passive state and off during the active state. Simultaneous high-time-resolution X-ray and radio observations in quiescence are thus highly desirable, in order to test this prediction and shed more light onto IGR J18245–2452’s unique properties. Measurements of the magnetic field and spin-down rate of PSR J1824–2452I will constrain the pulsar wind energy and may allow a quantitative estimate of the intrabinary shock properties (e.g., Bogdanov, Grindlay & van den Berg 2005).

Our proposed scenario implies that non-thermal magnetospheric emission can be quickly (within less than eight

minutes) and repeatedly (more than ten times in three days) quenched and reactivated, and that the intrabinary shock may form on similar timescales. Based on the morphology of the X-ray light curves from the MRP PSR J1023+0038, Bogdanov et al. (2011a) concluded that the intrabinary shock is localized near or at the surface of the companion star, close to the inner Lagrangian point. For IGR J18245-2452, the intra-binary shock during the passive state is probably much closer to the pulsar, where the pulsar wind runs into the inner boundary of the accretion disk (given the remarkably short time scales of switching between the passive and active states, it is unlikely that the wind blows most of the disk away and then irradiates the companion). Eventually, the pulsar wind might sweep the disk away leaving the system in a long-term “deep quiescence” state that resembles the other so-called “redback” radio MSP binaries. This is probably the state IGR J18245-2452 was in during the 2002 and 2006 *Chandra* observations.

Acknowledgments:

ML thanks M. Kachelrieß and the Norwegian U. of Science and Technology for their hospitality while part of this work was completed, and J. Casares and M. Roberts for stimulating discussions. RW is supported by an European Research Council starting grant. AP acknowledges support from the Netherlands Organization for Scientific Research (NWO) Vidi fellowship DA acknowledges support from the Royal Society. JH and DP acknowledge support by the National Aeronautics and Space Administration through Chandra Award Number GO3-14032B issued by the Chandra X-ray Observatory Center, which is operated by the Smithsonian Astrophysical Observatory for and on behalf of the National Aeronautics Space Administration under contract NAS8-03060. This research has made use of data and software provided by the High Energy Astrophysics Science Archive Research Center (HEASARC). The scientific results reported in this article are based in part on observations made by the Chandra X-ray Observatory and data obtained from the Chandra Data Archive. This work used Swift Gamma-ray Burst Explorer target-of-opportunity observations (PIs Ferrigno, Romano).

REFERENCES

- Alpar M. A., Cheng A. F., Ruderman M. A., Shaham J., 1982, *Nature*, 300, 728
- Archibald A. M., Kaspi V. M., Bogdanov S., Hessels J. W. T., Stairs I. H., Ransom S. M., McLaughlin M. A., 2010, *ApJ*, 722, 88
- Archibald A. M. et al., 2009, *Science*, 324, 1411
- Armas Padilla M., Degenaar N., Patruno A., Russell D. M., Linares M., Maccarone T. J., Homan J., Wijnands R., 2011, *MNRAS*, 417, 659
- Armas Padilla M., Degenaar N., Wijnands R., 2013, *MNRAS*
- Arnaud K. A., 1996, in *Astronomical Society of the Pacific Conference Series*, Vol. 101, *Astronomical Data Analysis Software and Systems V*, Jacoby G. H., Barnes J., eds., pp. 17–+
- Arons J., Tavani M., 1993, *ApJ*, 403, 249
- Backer D. C., Kulkarni S. R., Heiles C., Davis M. M., Goss W. M., 1982, *Nature*, 300, 615
- Bahramian et al., 2013, Submitted to *ApJ*
- Barthelmy S. D., Burrows D. N., D’Elia V., Holland S. T., Kennea J. A., Markwardt C. B., Marshall F. E., Palmer D. M., 2013, *GRB Coordinates Network*, 14355, 1
- Becker W. et al., 2003, *ApJ*, 594, 798
- Begin S., 2006, Master’s thesis, Faculty of Physics, UBC
- Bildsten L., 1998, in *NATO ASIC Proc. 515: The Many Faces of Neutron Stars.*, R. Buccheri, J. van Paradijs, & A. Alpar, ed., pp. 419–+
- Bogdanov S., Archibald A. M., Hessels J. W. T., Kaspi V. M., Lorimer D., McLaughlin M. A., Ransom S. M., Stairs I. H., 2011a, *ApJ*, 742, 97
- Bogdanov S., Grindlay J. E., van den Berg M., 2005, *ApJ*, 630, 1029
- Bogdanov S. et al., 2011b, *ApJ*, 730, 81
- Brown E. F., Bildsten L., Rutledge R. E., 1998, *ApJL*, 504, L95
- Burderi L., Di Salvo T., D’Antona F., Robba N. R., Testa V., 2003, *A&A*, 404, L43
- Campana S., Colpi M., Mereghetti S., Stella L., Tavani M., 1998, *A&ARv*, 8, 279
- Campana S., Stella L., 2003, *ApJ*, 597, 474
- Campana S. et al., 2002, *ApJL*, 575, L15
- Campana S., Stella L., Kennea J. A., 2008, *ApJL*, 684, L99
- Clark G. W., 1975, *ApJL*, 199, L143
- Cohn H. N., Lugger P. M., Bogdanov S., Heinke C. O., Van Den Berg M., Sivakoff G., 2013, *The Astronomer’s Telegram*, 5031, 1
- Corbel S., Tomsick J. A., Kaaret P., 2006, *ApJ*, 636, 971
- Degenaar N., Wijnands R., 2012, *MNRAS*, 422, 581
- Degenaar N., Wijnands R., Miller J. M., 2013, *ApJL*, 767, L31
- Eckert D. et al., 2013, *The Astronomer’s Telegram*, 4925, 1
- Esin A. A., McClintock J. E., Narayan R., 1997, *ApJ*, 489, 865
- Fruscione A. et al., 2006, in *Society of Photo-Optical Instrumentation Engineers (SPIE) Conference Series*, Vol. 6270, *Society of Photo-Optical Instrumentation Engineers (SPIE) Conference Series*
- Galloway D. K., Munro M. P., Hartman J. M., Psaltis D., Chakrabarty D., 2008, *ApJS*, 179, 360
- Gotthelf E. V., Kulkarni S. R., 1997, *ApJL*, 490, L161
- Haensel P., Zdunik J. L., 1990, *A&A*, 227, 431
- Haensel P., Zdunik J. L., 2008, *A&A*, 480, 459
- Harris W. E., 1996, *AJ*, 112, 1487
- Hasinger G., van der Klis M., 1989, *A&A*, 225, 79
- Heinke C. O., Bahramian A., Wijnands R., Altamirano D., 2013, *The Astronomer’s Telegram*, 4927, 1

- Heinke C. O., Grindlay J. E., Edmonds P. D., 2005, *ApJ*, 622, 556
- Heinke C. O., Jonker P. G., Wijnands R., Taam R. E., 2007, *ApJ*, 660, 1424
- Heinke C. O., Wijnands R., Cohn H. N., Lugger P. M., Grindlay J. E., Pooley D., Lewin W. H. G., 2006, *ApJ*, 651, 1098
- Hermesen W. et al., 2013, *Science*, 339, 436
- Homan J., Pooley D., 2013, *The Astronomer's Telegram*, 5086, 1
- Illarionov A. F., Sunyaev R. A., 1975, *A&A*, 39, 185
- in't Zand J. J. M., Jonker P. G., Markwardt C. B., 2007, *A&A*, 465, 953
- Kuulkers E., den Hartog P. R., in't Zand J. J. M., Verbunt F. W. M., Harris W. E., Cocchi M., 2003, *A&A*, 399, 663
- Lamb F. K., Pethick C. J., Pines D., 1973, *ApJ*, 184, 271
- Linares M., 2009, PhD thesis, Sterrenkundig Instituut "Anton Pannekoek" - University of Amsterdam
- Linares M., 2013, *The Astronomer's Telegram*, 4960, 1
- Narayan R., Yi L., 1995, *ApJ*, 452, 710
- Pallanca C., Dalessandro E., Ferraro R. F., Lanzoni B., Beccari G., 2013, *The Astronomer's Telegram*, 5003, 1
- Papitto A., Bozzo E., Ferrigno C., Pavan L., Romano P., Campana S., 2013a, *The Astronomer's Telegram*, 4959, 1
- Papitto A. et al., 2013b, *Nature*, 501, 517
- Papitto A. et al., 2013c, *The Astronomer's Telegram*, 5069, 1
- Patruno A., 2013, *The Astronomer's Telegram*, 5068, 1
- Patruno A., Watts A. L., 2012, *ArXiv e-prints* 1206.2727
- Patruno A., Watts A. L., Klein-Wolt M., Wijnands R., van der Klis M., 2009, *ApJ*, submitted; *ArXiv* 0904.0560
- Pavan L. et al., 2013, *The Astronomer's Telegram*, 4981, 1
- Plotkin R. M., Gallo E., Jonker P. G., 2013, *ArXiv e-prints*
- Pooley D. et al., 2003, *ApJL*, 591, L131
- Riggio A. et al., 2013, *The Astronomer's Telegram*, 5086, 1
- Romano P. et al., 2013, *The Astronomer's Telegram*, 4929, 1
- Rutledge R. E., Bildsten L., Brown E. F., Pavlov G. G., Zavlin V. E., 2000, *ApJ*, 529, 985
- Rutledge R. E., Bildsten L., Brown E. F., Pavlov G. G., Zavlin V. E., 2001, *ApJ*, 551, 921
- Rutledge R. E., Bildsten L., Brown E. F., Pavlov G. G., Zavlin V. E., Ushomirsky G., 2002, *ApJ*, 580, 413
- Servillat M., Heinke C. O., Ho W. C. G., Grindlay J. E., Hong J., van den Berg M., Bogdanov S., 2012, *MNRAS*, 423, 1556
- Sobolewska M. A., Papadakis I. E., Done C., Malzac J., 2011, *MNRAS*, 417, 280
- Soria R., Zampieri L., Zane S., Wu K., 2011, *MNRAS*, 410, 1886
- Stappers B. W., Gaensler B. M., Kaspi V. M., van der Klis M., Lewin W. H. G., 2003, *Science*, 299, 1372
- Testa V., Corsi C. E., Andreuzzi G., Iannicola G., Marconi G., Piersimoni A. M., Buonanno R., 2001, *AJ*, 121, 916
- Tsujimoto M. et al., 2011, *A&A*, 525, A25
- Wang Z., Archibald A. M., Thorstensen J. R., Kaspi V. M., Lorimer D. R., Stairs I., Ransom S. M., 2009, *ApJ*, 703, 2017
- Wijnands R., Degenaar N., Page D., 2013, *MNRAS*, 432, 2366
- Wijnands R., Heinke C. O., Pooley D., Edmonds P. D., Lewin W. H. G., Grindlay J. E., Jonker P. G., Miller J. M., 2005, *ApJ*, 618, 883
- Wijnands R., van der Klis M., 1998, *Nature*, 394, 344
- Wu Q., Gu M., 2008, *ApJ*, 682, 212
- Zampieri L., Turolla R., Zane S., Treves A., 1995, *ApJ*, 439, 849
- Zavlin V. E., 2007, *ApSS*, 308, 297